Elastic flow instability, curved streamlines, and mixing in microfluidic flows

Jai A. Pathak
National Institute of Standards and Technology, Polymers Division, Gaithersburg, Maryland 20899-8544

David Ross
National Institute of Standards and Technology, Process Measurements Division, Gaithersburg, Maryland 20899-8362

Kalman B. Migler
National Institute of Standards and Technology, Polymers Division, Gaithersburg, Maryland 20899-8544

(Received 10 December 2003; accepted 21 July 2004; published online 5 October 2004)

Flow instabilities are well known to occur in macroscopic flows when elastic fluids flow along curved streamlines. In this work we use flow visualization to study the mechanism underlying a purely elastic flow instability for Poiseuille flow in a *micro* (μ)*channel* having a zigzag path (curved streamlines) and quantitatively investigate its implications for fluid mixing (studied by fluorescence microscopy) in the μchannel. We find that the instability enhances mixing over the range of applied flow rates. For Newtonian streams, mixing occurs by molecular diffusion, and, as expected, mixing worsens with increasing flow rate because of decreasing residence time. However, for elastic fluid streams, we find substantial enhancement of mixing at sufficiently *high* throughputs, which indicates a strategy to counter the loss of diffusive mixing at high throughputs by exciting an elastic flow instability. Flow visualization is done using neutrally buoyant non-Brownian tracer particles added to the elastic fluids and also to the Newtonian fluids. In the Newtonian fluids, the tracer particles follow the streamlines. In the elastic fluids, the particles are *radially* displaced while flowing around bends in the zigzag μchannel, revealing the presence of secondary flow. This radial secondary flow, which promotes mixing between adjacent fluid streams, motivates us to draw an analogy between the instability observed here for the elastic fluids in the μchannel and the elastic instability that occurs in systems with curved streamlines, e.g., in the viscoelastic (non-inertial) Taylor–Couette, Dean, and Taylor–Dean instabilities. [DOI: 10.1063/1.1792011]

I. INTRODUCTION

It is well known that *purely elastic* flow instabilities[1,2] can occur in elastic fluids flowing along curved streamlines. The appropriate dimensionless parameters that govern the *onset* of these flow instabilities[3] (in terms of creating the nonlinearities in flow response) are the Weissenberg number (Wi) and the Deborah number (De).[4] Wi is the ratio of the first normal stress difference (N_1) to the shear stress (τ), which are both functions of shear rate ($\dot{\gamma}$). De is the dimensionless residence time:

$$\mathrm{Wi} = \frac{N_1(\dot{\gamma})}{\tau(\dot{\gamma})}, \tag{1}$$

$$\mathrm{De} = \frac{\lambda}{t_{res}}. \tag{2}$$

The symbol λ denotes the longest relaxation time of the polymer chains in the elastic fluid and t_{res} is the characteristic residence time of the flow. McKinley *et al.*[3] have considered purely elastic instabilities in several different geometries (Couette, cone-and-plate, eccentric cylinders, etc.) and derived dimensionless criteria, which combine the streamline curvature and the first normal stress difference, which can be used to identify critical conditions that govern the growth of these instabilities. It is also known that these instabilities are seen when $\varepsilon^{1/2}\mathrm{Wi} = O(1)$.[5] Here $\varepsilon = d/R_{curv}$ denotes the dimensionless radius of curvature, d is the gap width (e.g., between concentric cylinders in a Couette cell) and R_{curv} is the radius of curvature (taken to be the inner cylinder radius in the Couette setup). These instabilities are considered purely elastic as they occur at Reynolds number $\mathrm{Re} \ll 1$, or, equivalently, $\mathrm{Ta} \ll 1$, where $\mathrm{Ta} = \varepsilon \mathrm{Re}^2$ is the Taylor number.[6]

Since microfluidic flows are low Re flows, mixing of fluid streams in μchannels is diffusion limited. The characteristic time scale of molecular diffusion can often exceed the residence time of the fluid stream in a μchannel, requiring longer channels for mixing streams at high flow rates and/or species with small diffusion coefficients. Mixing of viscoelastic liquids (e.g., polymers)[7] poses a similar challenge faced in mixing fluids in microfluidic flows, as they are both low Re flows, and scientists[8,9] have explored the use of chaotic mixing/advection to promote mixing in viscoelastic liquids. Certainly, an alternative strategy for promoting mixing in μchannels would be chaotic advection. In this work we focus on exploiting purely elastic flow instabilities. Scientists have proposed different approaches to improve mixing in μchannels such as a three-dimensional serpentine μchannel for passive mixing,[10] three-dimensional microvascular networks,[11] placement of slanted wells at the junction of a T μchannel,[12] hydrodynamic focusing,[13] flow obstacles

in μchannels,[14] bas relief structures on the μchannel floor,[15] use of internal hydrodynamic recirculation in emulsion droplets under shear flow,[16] electrokinetic flow instabilities,[17,18] and electrohydrodynamic mixing.[19] Many of these approaches have been nicely discussed by Stone *et al.*[20] in their recent review on microfluidic flows.

While the nonlinear response of elastic fluids has been cleverly exploited for achieving fluidic control and memory elements in a μchannel,[21] to our knowledge, no study has been published hitherto on purely elastic flow instabilities in μchannels with curved streamlines, and their impact on the mixing of fluid streams. Groisman and Steinberg have published an experimental study on the effect of fluid elasticity on the mixing of streams in *macroscopic* curvilinear channels.[22] Their serpentine channel had a depth of 3 mm, and consisted of 60 smoothly interconnected half rings with inner and outer radii of 3 mm and 6 mm, respectively. While recent reports suggest that Burghelea *et al.* have extended this work to microchannels (see Ref. 16 in Ref. 23), it is not currently available in the published literature.

Here, we extend the work of Groisman and Steinberg to microfluidic channels. Beyond the practical applications, this scaling down of dimensions is of interest because microhydrodynamic flow[24] can be significantly affected by surface forces (surface tension), van der Waals forces, electrical charges, surface roughness, complicated three-dimensional geometry, and the possibility that suspended particles or dissolved polymer chains have dimensions comparable to those of the μchannels. Here we are also concerned with the crossover from diffusive mixing (at the smaller flow rates used) to mixing driven by fluid elasticity (at higher flow rates). Elasticity on its own is not sufficient for exciting these purely elastic flow instabilities, and we argue that these purely elastic flow instabilities come about due to coupling between curved streamlines and elasticity.[25] We note that Stone *et al.*[20] have also alluded to the use of elasticity as an approach to passive mixing by coupling elasticity with streamline curvature. Here we show that it is indeed possible to attain the critical value of $\varepsilon^{1/2}\mathrm{Wi}$ required to trigger a purely elastic instability in a μchannel and force mixing between adjacent fluid streams.

We carry out our mixing experiments with a model elastic fluid whose rheology and physical chemistry are well characterized. We prepare a model aqueous elastic fluid (a dilute polymer solution, essentially a Boger fluid[26,27]) having constant shear viscosity but appreciable elasticity (reflected in N_1). We excite a flow instability in the μchannel flow of this elastic fluid in regimes where $\mathrm{Wi}/\mathrm{Re} \gg 1$ and $\varepsilon^{1/2}\mathrm{Wi} = O(1)$. For the channel, ε is defined in terms of the channel width w: $\varepsilon = w/R_{curv}$. We compare mixing between fluid streams in the μchannel (quantified from fluorescence microscopy data) in the cases where both analyte streams are (a) Newtonian fluids and (b) elastic fluids. We elucidate the mechanism of the instability by visualization of tracer particle trajectories in the elastic fluids flowing in the μchannel.

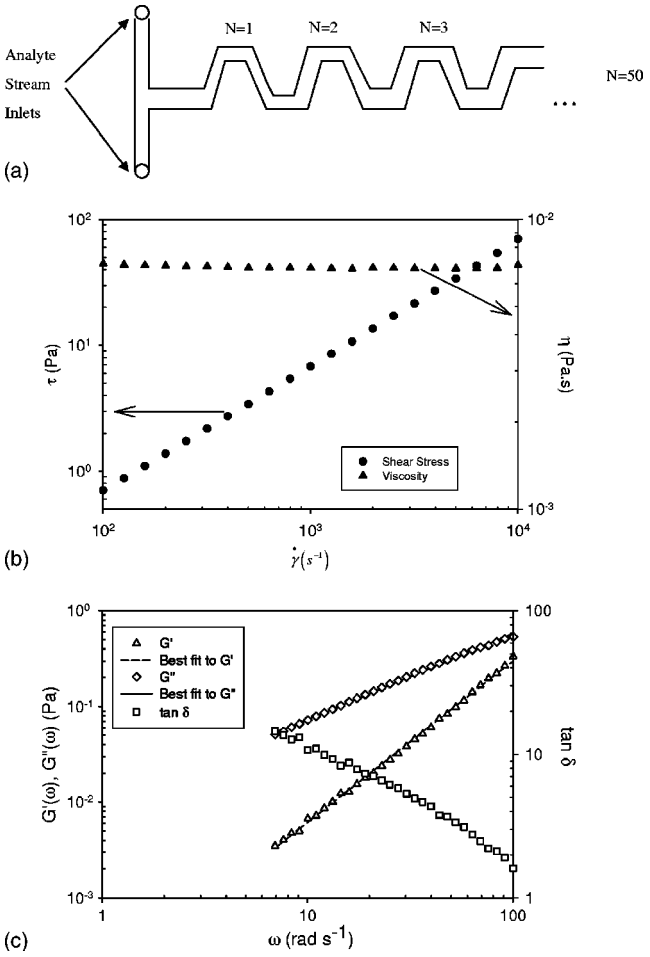

FIG. 1. (a) Schematic of the μchannel used in these experiments. (b) Steady shear rheology of the model aqueous elastic fluid. (c) Oscillatory shear rheology of the model aqueous elastic fluid.

II. EXPERIMENTAL PROCEDURE

A. Channel fabrication

A zigzag μchannel [see Fig. 1(a) for sketch] was fabricated by ablation of a polycarbonate substrate with a 193 nm UV excimer laser, and then sealed with a poly(methylmethacrylate) lid overnight in an oven at 105 °C (see Ref. 12 for details). Inlet ports for the analyte streams were drilled on the lid prior to sealing, and then syringe needles were placed in the ports and held in place by cured epoxy. The channel dimensions are width $w = 85$ μm, depth $d = 60$ μm and contour length $L = 45$ mm (from the junction of the analyte inlets to the outlet).

B. Preparation, rheological and physical characterization of Newtonian and elastic fluids

A solution of 39.15% mass fraction sucrose and 0.6% mass fraction sodium chloride was prepared in de-ionized water as the control Newtonian fluid. An elastic solution containing 6.6×10^{-3}% mass fraction polyacrylamide (PA) of mass average molar mass $(M) = 1.8 \times 10^7$ (Polysciences)[28] was prepared in the Newtonian fluid. The PA concentration was kept well below the overlap concentration[29] $c^* (\cong 1/[\eta])$ where $[\eta]$ is the intrinsic viscosity, to make a

dilute polymer solution. We fit the data of Kulicke *et al.*[30] on M dependence of $[\eta]$ to the Mark–Houwink equation[31] $[\eta]=KM^a$, to determine the Mark–Houwink coefficients $K(=1.46\times10^{-2}$ L/kg) and $a(=0.72)$ for polyacrylamide in water. The value of a is in accord with our expectations for a good solvent $(0.7<a<0.8)$.[31] These Mark–Houwink constants are also in fair agreement with those provided by Kurata and Tsunashima.[32] We used this Mark–Houwink equation to estimate the intrinsic viscosity of our aqueous PA solution at room temperature, $[\eta]=2.4\times10^3$ L/kg, and this the overlap concentration $c^*=4.1\times10^{-4}$ kg L^{-1}. Since $[\eta]\approx R^3/M\approx1/c^*$, we estimate the size of the chains $R\cong0.4$ μm. This value of R is consistent with dimensions of PA chains of comparable molar mass, as listed by Kulicke *et al.*[30] The PA chains are much smaller than the channel dimensions and finite size effects on the polymer dynamics are unambiguously ruled out.

Sucrose was added to increase the solution viscosity and thus boost the longest relaxation time of the PA chains therein. Sodium chloride was added to the solution with a view to making electro-osmotic flow (EOF) measurements, but we used Poiseuille flow since EOF gives much lower volumetric flow rates (Q) than Poiseuille flow. Achieving sufficiently high Q, and, hence, high $\dot\gamma$, which enable us to reach the regime where $\mathrm{Wi}>1$, is of paramount importance for triggering the elastic instability. The solution viscosities (measured using 50 mm diameter cone-plate tools with 0.04 rad cone angle in a Rheometric Scientific ARES rheometer equipped with a low shear Force Rebalance Transducer) are $\eta=5.9\times10^{-3}$ Pa s (Newtonian fluid) and $\eta=6.8\times10^{-3}$ Pa s (elastic fluid) at 22 °C. Thus, the viscosity η of the elastic fluid was quite insignificantly perturbed over the viscosity of the Newtonian fluid. The steady shear rheology of the elastic fluid is shown in Fig. 1(b).

Linear viscoelastic measurements of the angular-frequency (ω)-dependent complex shear modulus, $G^*(\omega)=G'(\omega)+iG''(\omega)$, were made on the elastic fluid at 23 °C [see Fig. 1(c)]. The elastic fluid exhibits classical terminal response[33] of a viscoelastic liquid under these conditions, as G'' exceeds G' over all accessible frequencies. The exact terminal slopes ($G'\sim\omega^2$ and $G''\sim\omega$) are not seen due to the polydispersity of the PA chains. The longest relaxation time (Zimm time) of the polymer chains is estimated by fitting the best-fit straight lines to G' and G'', and extrapolating them to determine where the best-fit lines intersect (see Fig. 8.7 in Ref. 31). The frequency ω_c corresponding to the intersection serves as a measure of the longest Zimm relaxation time. We determined $\omega_c\cong160$ rad s^{-1} and thus the longest relaxation time for the PA chains in the elastic fluid $\lambda=1/\omega_c=6.25\times10^{-3}$ s. No fluid inertia effects were seen, as we operate in the so-called gap-loading limit, where the rheometer gap h is much smaller than the shear wavelength λ_{shear}. We estimated λ_{shear} from our data using its relation to $G^*(\omega)$ and the phase angle (δ): $\lambda_{shear}=2\pi/[\omega\sqrt{(\rho/G_d)}\cos(\delta/2)]$, where ρ denotes fluid density and G_d is defined by the relation $G'=G_d\sin\delta$, or, $G''=G_d\cos\delta$. Schrag[34] has shown that when $h\ll\lambda_{shear}$ in the gap-loading limit, the shear wave propagates across the gap without damping and fluid inertia effects are negligible. From our data, we determine $0.017<h/\lambda_{shear}<0.033$.

The viscoelasticity of Boger fluids and dilute polymer solutions is captured by the Oldroyd-B[4,35] constitutive equation, derived by treating the polymer chain as a dumbbell where two frictional beads are connected by a Hookean spring. The stress tensor $\boldsymbol{\tau}=\boldsymbol{\tau}_p+\boldsymbol{\tau}_s$ is the sum of the polymer stress $\boldsymbol{\tau}_p$ and solvent stress $\boldsymbol{\tau}_s=-\eta_s\dot\gamma$. The term η_s is the solvent viscosity and $\dot\gamma=\nabla\mathbf{v}+\nabla\mathbf{v}^{\mathbf{T}}$ is the rate of strain tensor (the superscript $\mathbf{T}$ denotes the transpose of the tensor obtained from the gradient of the velocity vector $\mathbf{v}$). The solution viscosity η is $\eta=\eta_s+\eta_p$, where η_p is the polymer viscosity. The $\boldsymbol{\tau}_p$ is written as follows:

$$\boldsymbol{\tau}_p+\lambda_d\boldsymbol{\tau}_{p(1)}=-\eta_p\dot\gamma. \tag{3}$$

Here λ_d is the dumbbell relaxation time and $\boldsymbol{\tau}_{p(1)}$ is the convected derivative of $\boldsymbol{\tau}_p$.

$$\boldsymbol{\tau}_{p(1)}=\frac{D}{Dt}(\boldsymbol{\tau}_p)-[\boldsymbol{\tau}_p\cdot\nabla\mathbf{v}+\nabla\mathbf{v}^{\mathbf{T}}\cdot\boldsymbol{\tau}_p]. \tag{4}$$

$D/Dt=d/dt+\mathbf{v}\cdot\nabla$ denotes the substantial derivative in the Eulerian frame. Bird *et al.*[4] have evaluated the shear stress and the first normal stress difference for the Oldroyd-B fluid:

$$\begin{aligned}\tau&=\tau_{21}=-\eta\dot\gamma,\\ N_1&=\tau_{11}-\tau_{22}=-2\eta\lambda_d\dot\gamma^2.\end{aligned} \tag{5}$$

Applying the results in Eq. (5) to Eq. (1) yields $\mathrm{Wi}=2\lambda_d\dot\gamma$. We shall invoke these characteristics of the Oldroyd-B fluid when we discuss the physics underlying the instability observed in this work.

C. Fluorescence microscopy and quantification of mixing

The control experiment involved mixing of the Newtonian fluid in both analyte streams, with Rhodamine B (Acros Organics) dye added to one stream as a fluorescent probe to visualize flow, and quantifying mixing in the μchannel. The dye concentration was kept sufficiently small $(1.1\times10^{-4}$ mol/L) to prevent self-quenching. The gain on the detector was set carefully to prevent saturation of pixel intensities. Fluorescence microscopy (543 nm He–Ne laser) was performed on a Zeiss LSM 510 confocal laser-scanning microscope. The next experiment involved quantifying mixing of two streams, each containing the elastic fluid, with Rhodamine B added to one of the two streams. Poiseuille flow, generated by a syringe pump, was used to set the analyte stream flow rates.

Quantification of the deviation from mixing D_i is based on a metric proposed by Liu *et al.*,[10]

$$D_i=\sqrt{\frac{1}{N}\sum_{i=1}^{N}(I_i-I_{\max})^2}. \tag{6}$$

N denotes the number of pixels; I_i and $I_{\max}$ denote the intensity at pixel i and the maximum intensity, respectively, observed at any pixel in a fully mixed system. D_i was calculated at several points along the channel, and normalized by the value of D_i at the channel junction where the incoming analyte streams meet. It follows from Eq. (2) and the nor-

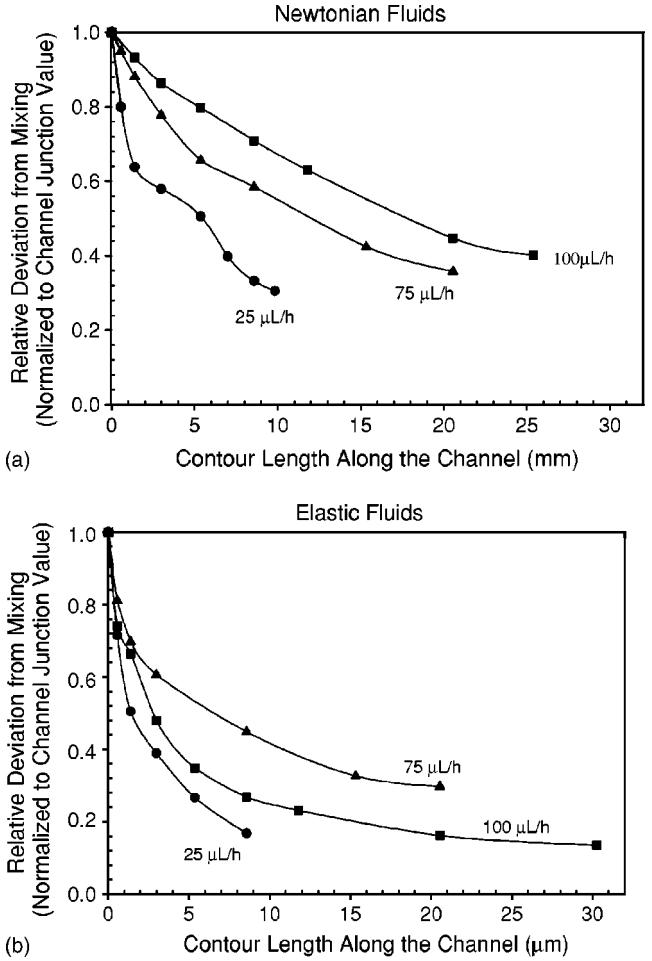

FIG. 2. Deviation from mixing between (a) Newtonian analyte streams and (b) elastic analyte streams in the μchannel. The deviation from mixing is normalized by the corresponding value at the channel junction. Lines merely guide the eye.

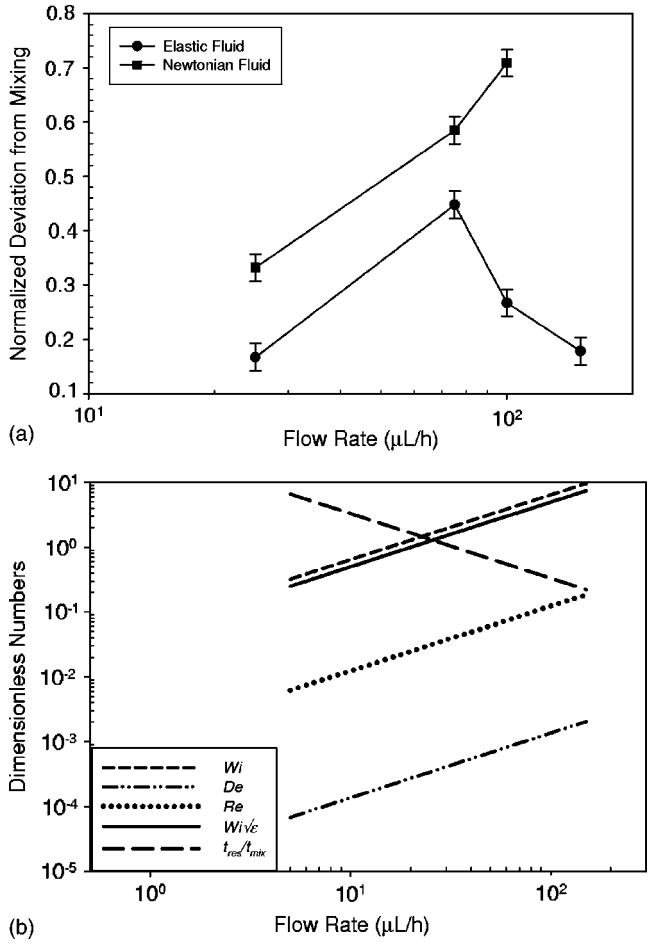

FIG. 3. (a) Comparison of the deviation from mixing vs volumetric flow rate between the elastic and the Newtonian cases, at a fixed point (8.5 mm from the stream junction). Lines merely guide the eye. The bars are a measure of the typical standard uncertainty associated with the data in Figs. 2(a), 2(b), and 3(a), and numerically equal one standard deviation. (b) The dimensionless numbers Wi, Wi/$\varepsilon^{1/2}$, De, Re, and t_{res}/t_{mix} plotted vs Q.

malization that for two perfectly mixed streams $D_{i,normalized}=0$, while for two completely unmixed streams $D_{i,normalized}=1$.

III. RESULTS AND DISCUSSIONS

The comparison of the deviation from mixing between Newtonian streams and elastic streams is shown in Figs. 2(a) and 2(b), respectively. Data are shown in Fig. 2 for 25 μL/h, 75 μL/h, and 100 μL/h. For the elastic fluid only, Q was pushed up to 150 μL/h. For all Q studied, the $D_{i,normalized}$ is smaller in the elastic fluids than in the Newtonian fluids, indicating an enhancement of mixing with elasticity. As expected, the $D_{i,normalized}$ at any spot on the channel increases with increasing Q for the Newtonian fluids, due to decreasing t_{res} as $t_{res}\sim Q^{-1}$. In contrast, for the elastic fluids, the relationship between Q and $D_{i,normalized}$ is not strictly monotonic: compare the order of the curves in Figs. 2(a) and 2(b). This is also seen clearly in Fig. 3(a), where a comparison of $D_{i,normalized}$ vs Q in the two cases is made at a fixed spot, 8.5 mm from the junction of the analyte streams.

For the elastic fluids, the interesting result of the peak in the $D_{i,normalized}$ vs Q curve in Fig. 3(a) arises due to the competition between residence time and elastic instability effects. To understand this result, we calculate Wi, $\varepsilon^{1/2}$Wi, Re, and De [see Fig. 3(b)] for the flow of the elastic fluid in the μchannel. The residence time $t_{res}=L/\langle v\rangle$, where $\langle v\rangle$ is the average velocity. As an engineering approximation, we assumed the channel to be nearly circular in cross section and calculated an average $\dot{\gamma}=4Q/d^3$, for calculating Wi. The ratio Wi/Re$\cong$52 for our system signifies (in conjunction with Wi$>$1 and Re$\ll$1) that inertial effects are negligible and significant chain stretching occurs.

Using the molecular diffusion time estimate $t_{mix}\cong w^2/D$, we determine $t_{mix}\cong 14$ s (using the diffusion coefficient $D\cong 10^{-10}$ m^2 s^{-1} known for Fluoroscein, a molecule similar to Rhodamine B). Residence time effects are important at 25 μL/h [$t_{mix}/t_{res}\cong 0.75$ at 25 μL/h; see Fig. 3(b)] for the Newtonian streams: the streams spend long enough in the channel for diffusion to provide appreciable mixing. On the other hand, for the elastic fluid at $Q=25$ μL/h, both the advantageous effects of large residence time *and* the incipient elastic flow instability ($\varepsilon^{1/2}$Wi$\cong 1$) are felt. With increasing Q, the effects of residence time are progressively lost (e.g., at $Q=75$ μL/h, $t_{mix}/t_{res}\cong 2.2$) while the effects from the flow instability are increasingly felt, giving rise to a peak

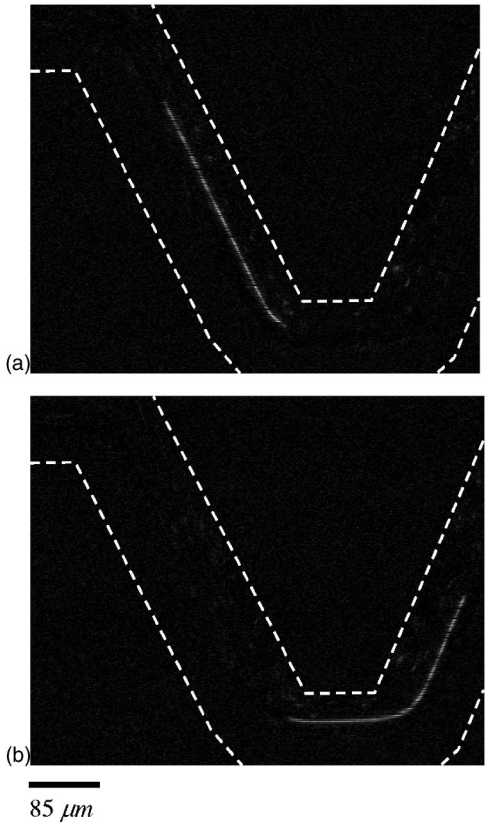

FIG. 4. Position of tracer particle streak in elastic fluid in the μchannel observed at (a) time t and (b) at time $t+0.03$ s. The dashed lines are drawn to indicate the channel edges. The background (containing tracer particles stuck to the walls of the channel) was subtracted, so that only the position of the streak is visible in the image. Data were taken at a flow rate of 50 μL/h.

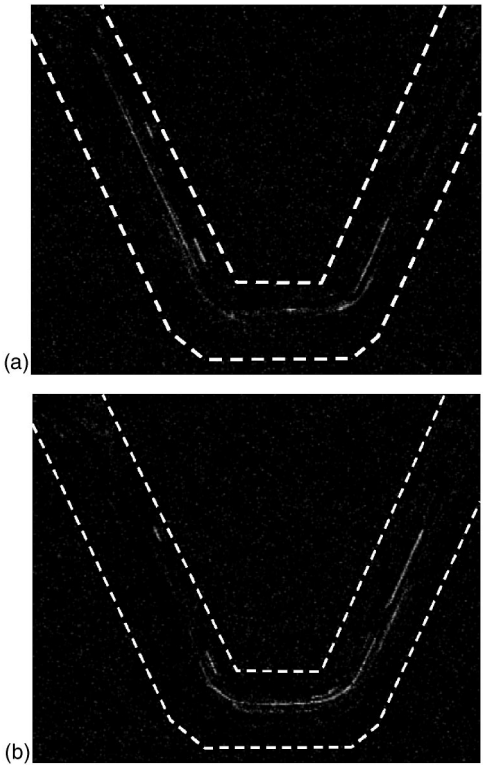

FIG. 5. Position of tracer particle streaks in Newtonian fluid in the μchannel observed at (a) time t and (b) at time $t+0.03$ s. The dashed lines are drawn to indicate the channel edges. The background (containing tracer particles stuck to the walls of the channel) was subtracted, so that only the position of the streaks is visible in the image. Scale bar from Fig. 4 also applies to Fig. 5. Data were taken at a flow rate of 50 μL/h.

in the curve of $D_{i,normalized}$ vs Q for the *elastic* fluid streams. Ultimately, the flow instability effects become sufficiently strong on their own to counter the decreased residence time at higher Q, and then $D_{i,normalized}$ decreases steadily with increasing Q (i.e., increasing Wi).

What causes the improved mixing in the elastic streams, kinematically? To gain insight into the mechanism of the underlying elastic flow instability, we performed flow visualization of tracer particles (Fluoresbrite polystyrene microspheres, Polysciences; average diameter$=0.5$ μm; concentration$=2.6\times10^{-3}$% mass fraction) added to the streams. The particles are effectively neutrally buoyant and the Peclét number ($\mathrm{Pe}=\dot{\gamma}r^2/D_{self}\approx\eta\dot{\gamma}r^3/kT$) associated with them is $\mathrm{Pe}=O(10^7)$, signifying the domination of convection over Brownian motion. D_{self} denotes the self-diffusion coefficient of the particle, r is the particle radius, k is Boltzmann's constant and T is absolute temperature. In the elastic streams [see Figs. 4(a) and 4(b); flow rate$=50$ μL/h], the tracer particles are radially displaced across the channel contours as they traverse a bend in the μchannel. In Fig. 4(a), the particle path (in that frame) is closer to the upper wall as it comes to the bend, while in the next frame [0.03 s later; Fig. 4(b)] it is closer to the lower wall. If d_1 denotes the distance of the streak from the top wall in the straight part of the bend, and d_2 denotes the distance of the streak from the top wall in the upturn section of the bend, then the data in Fig. 4(b) yield $d_2/d_1=1.4$. Visualization at a higher flow rate (100 μL/h) reveals that this value of d_2/d_1 increases to 2.4. Clearly, the magnitude of this radial displacement depends on Wi. While secondary flow (as discerned from the radial displacement of the streak while it traverses the bend in the channel) is clearly seen in the flow of elastic fluids in the μchannel, no such secondary motion is displayed by the tracer particle streaks when both fluid streams are Newtonian. In the Newtonian fluids, the particle paths follow the streamlines. In Figs. 5(a) and 5(b), we show the positions of particle streaks (visualized in the same location as Fig. 4; flow rate$=50$ μL/h) in two successive frames. The streaks in the Newtonian fluid follow the channel contours, and no radial displacement is seen.

Since this radial secondary motion (observed at various different bends in the μchannel) is a known characteristic of flow instabilities in elastic fluids flowing along curved streamlines, we are inspired to draw an analogy between the elastic flow instability observed in the μchannel and the instabilities observed for elastic fluids in Taylor–Couette,[36–39] Dean and Taylor–Dean flows.[40–42] This instability depends on a complex coupling between N_1 and curved streamlines. It seems that streamline curvature is an essential condition for the instability, as it has been concluded on the basis of analysis that non-inertial viscoelastic plane Couette flow is stable at all Wi.[43–45] For our channel we estimate $\varepsilon\cong0.60$ (the average radius of curvature was evaluated at the channel cen-

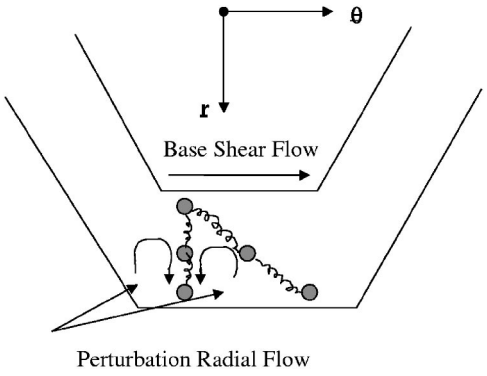

FIG. 6. Schematic of the axisymmetric mode of the instability in the flow of the elastic fluid in the Taylor–Couette setup (adapted from Ref. 36).

terline). When mapped back to the Taylor–Couette experimental setup,[36] this value of ε would correspond to the large gap case. The critical shear rate for the onset of the transition decreases with increasing ε.[37]

It has been well known since the 1960s that the second normal stress difference ($N_2=\tau_{22}-\tau_{33}$) is responsible for the development of secondary motions in viscoelastic flows through nonaxisymmetric channels.[4] Larson[1] has pointed out that shear thinning and a nonzero N_2 are predicted to have strong influences on the stability of viscoelastic flows, rendering the stability characteristics of dilute solutions significantly different from those of polymer melts. We can decisively rule out this as the mechanism for the observed secondary motion because N_2 is vanishingly small in dilute polymer solutions.[46] Magda *et al.*[46] have measured N_2 in a Boger fluid of polyisobutylene dissolved in polyisobutene and found its magnitude to be at least 30 times smaller than N_1, and opposite in sign. Since Boger fluids, by definition, do not shear thin, no influences of shear thinning are expected on the instability observed here.

As pointed out by Larson, Shaqfeh, and Muller in their seminal paper,[36] and further expounded by Groisman and Steinberg,[39] the axisymmetric mode of the instability (see sketch in Fig. 6) involves a radial extensional flow as a perturbation to the base (primary) shear flow. While Larson *et al.* considered this extensional flow to be time dependent, Groisman and Steinberg treated it as being time independent. We shall now summarize the arguments of Groisman and Steinberg[39] to rationalize the observed radial secondary flow.

The base (primary) flow in the system is a pressure-driven shear flow. The secondary flow involves a radial *extensional* flow (see Fig. 6) where $v_r=v_r(r)$ and the perturbation extensional rate is $\dot{\varepsilon}=\partial v_r/\partial r$. The rate of deformation tensor is then written as follows in the (r,θ,z) coordinate system:

$$\nabla \mathbf{v}=\begin{pmatrix} 0 & 0 & 0 \\ \dot{\gamma}_r & \dot{\varepsilon} & 0 \\ 0 & 0 & -\dot{\varepsilon} \end{pmatrix}. \tag{7}$$

When the rate of deformation tensor [Eq. (7)] is substituted in Eq. (3), then the following equations are obtained for $\boldsymbol{\tau}_p$. The sign convention of Bird *et al.*[4] is followed:

$$\tau_{\theta\theta}+\lambda_d\frac{d\tau_{\theta\theta}}{dt}=2\lambda_d\tau_{rr}\dot{\gamma}_{r\theta}, \tag{8}$$

$$\tau_{r\theta}+\lambda_d\frac{d\tau_{r\theta}}{dt}=\lambda_d\tau_{rr}\dot{\gamma}_{r\theta}+\lambda_d\tau_{r\theta}\dot{\varepsilon}-\eta_p\dot{\gamma}_{r\theta}, \tag{9}$$

$$\tau_{rr}+\lambda_d\frac{d\tau_{rr}}{dt}=2\lambda_d\tau_{rr}\dot{\varepsilon}-2\eta_p\dot{\varepsilon}. \tag{10}$$

If we assume that the perturbation is steady, i.e., $d\tau_{rr}/dt=0$, and that the term $\lambda_d\dot{\varepsilon}\ll 1$, then we get $\tau_{rr}=-2\eta_p\dot{\varepsilon}$. Since τ_{rr} and $\dot{\gamma}_{r\theta}$ are coupled to each other [see Eq. (9)], the stretching of the chains makes them increasingly susceptible to the base shear flow. The shear stress thus increases by $\Delta\tau_{r\theta}=-3\eta_p\dot{\varepsilon}\lambda_d\dot{\gamma}_{r\theta}$, which couples to $\dot{\gamma}_{r\theta}$ and causes an increase in the azimuthal (hoop) stress by $\Delta\tau_{\theta\theta}=-6\eta_p\dot{\varepsilon}(\lambda_d\dot{\gamma}_{r\theta})^2$. Since N_1 in the base shear flow is $N_1=\tau_{\theta\theta}-\tau_{rr}=-2\eta_p\lambda_d(\dot{\gamma}_{r\theta})^2$, the first normal stress difference increases by $\Delta N_1=\Delta\tau_{\theta\theta}-\tau_{rr}=-2\eta_p\dot{\varepsilon}[3(\lambda_d\dot{\gamma}_{r\theta})^2-1]$ due to the perturbation. This increase in azimuthal stress (and hence in N_1) drives the radial flow, and serves to improve mixing between the elastic fluid streams in the μchannel by increasing the area in contact between the streams and thus facilitating diffusion.

ACKNOWLEDGMENTS

The authors thank Dr. Laurie Locascio (Analytical Chemistry Division, NIST) for use of facilities in her group and Professor Michael Graham (University of Wisconsin), Professor Satish Kumar (University of Minnesota), and Dr. Steven Hudson (NIST) for helpful discussions and comments on the manuscript.

[1] R. G. Larson, "Instabilities in viscoelastic flows," Rheol. Acta **31**, 213 (1992).
[2] E. S. G. Shaqfeh, "Purely elastic instabilities in viscometric flows," Annu. Rev. Fluid Mech. **28**, 129 (1996).
[3] G. H. McKinley, P. Pakdel, and A. Öztekin, "Rheological and geometric scaling of purely elastic flow instabilities," J. Non-Newtonian Fluid Mech. **67**, 19 (1996).
[4] R. B. Bird, R. C. Armstrong, and O. Hassager, *Dynamics of Polymeric Liquids: Volume 1, Fluid Mechanics* (Wiley, New York, 1987).
[5] M. D. Graham, "Effect of axial flow on viscoelastic Taylor–Couette instability," J. Fluid Mech. **360**, 341 (1998).
[6] P. G. Drazin and W. H. Reid, *Hydrodynamic Instability* (Cambridge University Press, Cambridge, 1981).
[7] J. M. Ottino, *The Kinematics of Mixing: Stretching, Chaos and Transport* (Cambridge University Press, Cambridge, 1989).
[8] S. Kumar and G. M. Homsy, "Chaotic advection in creeping flow of viscoelastic fluids between slowly modulated eccentric cylinders," Phys. Fluids **8**, 1774 (1996).
[9] Y. Fan, R. I. Tanner, and N. Phan-Thien, "A numerical study of viscoelastic effects in chaotic mixing between eccentric cylinders," J. Fluid Mech. **412**, 197 (2000).
[10] R. H. Liu, M. A. Stremler, K. V. Sharp, M. G. Olsen, J. G. Santiago, R. J. Adrian, H. Aref, and D. J. Beebe, "Passive mixing in a 3 dimensional serpentine microchannel," J. Microelectromech. Syst. **9**, 190 (2000).
[11] D. Therriault, S. R. White, and J. A. Lewis, "Chaotic mixing in three-dimensional microvascular networks fabricated by direct-write assembly," Nat. Mater. **2**, 265 (2003).
[12] T. J. Johnson, D. Ross, and L. E. Locascio, "Rapid microfluidic mixing," Anal. Chem. **74**, 45 (2002).
[13] J. B. Knight, A. Vishwanath, J. P. Brody, and R. H. Austin, "Hydrodynamic focusing on a silicon chip: Mixing nanoliters in microseconds," Phys. Rev. Lett. **80**, 3863 (1998).
[14] H. Wang, P. Iovenitti, E. Harvey, and S. Masood, "Optimizing layout of

obstacles for enhanced mixing in microchannels," Smart Mater. Struct. **11**, 662 (2002).
[15]A. D. Stroock, S. K.W. Dertinger, A. Ajdari, I. Mezić, H. A. Stone, and G. M. Whitesides, "Chaotic mixer for microchannels," Science **295**, 647 (2002).
[16]J. D. Tice, H. Song, A. D. Lyon, and R. F. Ismagilov, "Formation of droplets and mixing in multiphase microfluidics at low values of the Reynolds and capillary numbers," Langmuir **19**, 9127 (2003).
[17]M. H. Oddy, J. G. Santiago, and J. C. Mikkelsen, "Electrokinetic instability micromixing," Anal. Chem. **73**, 5822 (2001).
[18]H. Lin, B. D. Storey, M. H. Oddy, C.-H. Chen, and J. G. Santiago, "Instability of electro-kinetic microchannel flows with conductivity gradients," Phys. Fluids **16**, 1922 (2004).
[19]C. Tsouris, C. T. Culbertson, D. W. DePaoli, S. C. Jacobson, V. F. de Almeida, and J. M. Ramsey, "Electrohydrodynamic mixing in microchannels," AIChE J. **49**, 2181 (2003).
[20]H. A. Stone, A. D. Stroock, and A. Ajdari, "Engineering flows in small devices: Microfluidics toward a lab-on-a-chip," Annu. Rev. Fluid Mech. **36**, 381 (2004).
[21]A. Groisman, M. Enzelberger, and S. R. Quake, "Microfluidic memory and control devices," Science **300**, 955 (2003).
[22]A. Groisman and V. Steinberg, "Efficient mixing at low Reynolds numbers using polymer additives," Nature (London) **410**, 905 (2001).
[23]T. Burghelea, E. Segre, and V. Steinberg, "Mixing by polymers: Experimental test of decay regime of mixing," Phys. Rev. Lett. **92**, 164501 (2004).
[24]H. A. Stone and S. Kim, "Microfluidics: Basic issues, applications and challenges," AIChE J. **47**, 1250 (2001).
[25]P. Pakdel and G. H. McKinley, "Elastic instability and curved streamlines," Phys. Rev. Lett. **77**, 2459 (1996).
[26]D. V. Boger, "Highly elastic constant-viscosity fluid," J. Non-Newtonian Fluid Mech. **3**, 87 (1977).
[27]D. V. Boger and R. Binnington, "Separation of elastic and shear thinning effects in the capillary rheometer," Trans. Soc. Rheol. **21**, 515 (1977).
[28]Certain commercial materials and equipment are identified in this paper in order to adequately specify the experimental procedure. In no case does such identification imply recommendation or endorsement by the National Institute of Standards and Technology, nor does it imply that these are necessarily the best available for the purpose.
[29]P. G. deGennes, *Scaling Concepts in Polymer Physics* (Cornell University Press, Ithaca, NY, 1979).
[30]W. M. Kulicke, M. Koetter, and H. Graeger, "Drag reduction phenomenon with special emphasis on polymer solutions," Adv. Polym. Sci. **89**, 1 (1989).
[31]M. Rubinstein and R. H. Colby, *Polymer Physics* (Oxford University Press, New York, 2003).
[32]M. Kurata and Y. Tsunashima, *Polymer Handbook* (Wiley, New York, 1999), Chap. VII/1, p. 1.
[33]J. D. Ferry, *Viscoelastic Properties of Polymers*, 3rd ed. (Wiley, New York, 1980).
[34]J. L. Schrag, "Deviation of velocity gradient profiles from the 'gap loading' and 'surface loading' limits in dynamic simple shear experiments," Trans. Soc. Rheol. **21**, 399 (1977).
[35]R. G. Larson, *Constitutive Equations for Polymer Melts and Solutions* (Butterworths, Boston, 1988).
[36]R. G. Larson, E. S. G. Shaqfeh, and S. J. Muller, "A purely elastic instability in Taylor–Couette flow," J. Fluid Mech. **218**, 573 (1990).
[37]E. S. G. Shaqfeh, S. J. Muller, and R. G. Larson, "The effects of gap width and dilute solution properties on the viscoelastic Taylor–Couette instability," J. Fluid Mech. **235**, 285 (1992).
[38]B. M. Baumert and S. J. Muller, "Flow visualization of the elastic Taylor–Couette instability in Boger fluids," Rheol. Acta **34**, 147 (1995).
[39]A. Groisman and V. Steinberg, "Mechanism of elastic instability in Couette flow of polymer solutions: Experiment," Phys. Fluids **10**, 2451 (1998).
[40]Y. L. Joo and E. S. G. Shaqfeh, "Viscoelastic Poiseuille flow through a curved channel—A new elastic instability," Phys. Fluids A **3**, 1691 (1991).
[41]Y. L. Joo and E. S. G. Shaqfeh, "A purely elastic instability in Dean and Taylor–Dean flow," Phys. Fluids A **4**, 524 (1992).
[42]Y. L. Joo and E. S. G. Shaqfeh, "Observations of purely elastic instabilities in the Taylor–Dean flow of a Boger fluid," J. Fluid Mech. **262**, 27 (1994).
[43]V. A. Gorodtsov and A. I. Leonov, "On a linear instability of a plane parallel Couette flow of a viscoelastic fluid," J. Appl. Math. Mech. **31**, 310 (1967).
[44]M. Renardy, "A rigorous stability proof for plane Couette-flow of an upper convected Maxwell fluid at zero Reynolds-number," Eur. J. Mech. B/Fluids **11**, 511 (1992).
[45]M. Renardy and Y. Renardy, "Linear-stability of plane Couette-flow of an upper convected Maxwell fluid," J. Non-Newtonian Fluid Mech. **22**, 23 (1986).
[46]J. J. Magda, J. Lou, S. G. Baek, and K. L. DeVries, "Second normal stress difference of a Boger fluid," Polymer **32**, 2000 (1991).